

# X-ray Spectroscopy of a Rare-Earth Molecular System Measured at the Single Atom Limit at Room Temperature

Sarah Wieghold,\* Nozomi Shirato, Xinyue Cheng, Kyaw Zin Latt, Daniel Trainer, Richard Sottie, Daniel Rosenmann, Eric Masson, Volker Rose, and Saw Wai Hla\*



Cite This: *J. Phys. Chem. C* 2023, 127, 20064–20071



Read Online

ACCESS |



Metrics & More

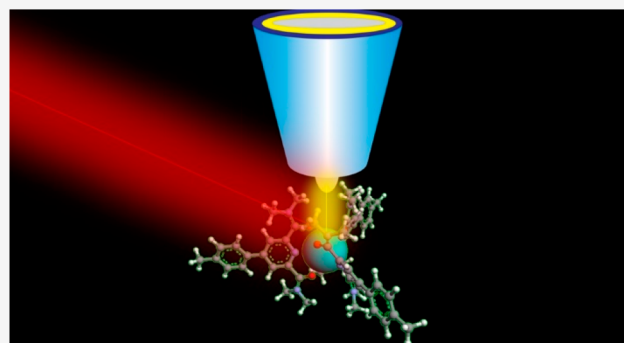


Article Recommendations



Supporting Information

**ABSTRACT:** We investigate the limit of X-ray detection at room temperature on rare-earth molecular films using lanthanum and a pyridine-based dicarboxamide organic linker as a model system. Synchrotron X-ray scanning tunneling microscopy is used to probe the molecules with different coverages on a HOPG substrate. X-ray-induced photocurrent intensities are measured as a function of molecular coverage on the sample, allowing a correlation of the amount of La ions with the photocurrent signal strength. X-ray absorption spectroscopy shows cogent  $M_{4,5}$  absorption edges of the lanthanum ion originated by the transitions from the  $3d_{3/2}$  and  $3d_{5/2}$  to  $4f$  orbitals. X-ray absorption spectra measured in the tunneling regime further reveal an X-ray excited tunneling current produced at the  $M_{4,5}$  absorption edge of the La ion down to the ultimate atomic limit at room temperature.



## INTRODUCTION

Rare-earth metals exhibit promising optical, magnetic, and catalytic properties and are used in a wide variety of energy conversion applications and quantum technologies including photon upconversion,<sup>1–3</sup> quantum cutting,<sup>4,5</sup> memory storage,<sup>6,7</sup> and quantum networks.<sup>8,9</sup> Rare-earth atoms doped or implanted as “defects” into a host crystal were demonstrated to exhibit long spin coherence and lifetimes,<sup>10,11</sup> narrow optical transitions, and the Laporte forbidden transition<sup>12,13</sup> owing to their unique electronic configuration of the  $4f$ -shell electrons. Despite these unique properties, one drawback is related to the fabrication of defect centers with spatial control and selectivity. Recently, molecular systems such as coordination complexes, metal–organic frameworks, and supramolecular networks have attracted attention due to their potential to precisely control the location and local environment of the rare-earth atoms by incorporating them into molecular scaffolds.<sup>14–16</sup> These molecular approaches provide tantalizing engineering control in which the properties and functionalities of rare-earth metal ions can be tailored for specific applications.<sup>17</sup> For example, helicates, cages, or cubes have been used as building blocks for extended and well-designed molecular systems by employing tridentate ligands based on pyridine-diamide and -dicarbonyl or carboxylic acid chelating moieties.<sup>18–20</sup> Rare-earth-based molecular systems can also be used to control the distance between electron and nuclear spin qubits by changing the length of the organic linkers, allowing the rate and efficiency of coherence transfer between them to be tuned.<sup>17</sup> By

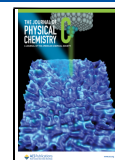
introducing functionalized groups via  $C\equiv C$  or  $C\equiv N$  bridges to the linker moiety embedded into the molecular systems, even vibrational modes can be added to modulate the coherence time.<sup>17,21</sup> Additionally, due to the multimodality of the linkers based on their design, a variety of lanthanide (Ln) atoms can be placed with atomic precision into molecular systems enabling access to various possible spin states as well as providing synthetic opportunities for potential applications in emission, energy upconversion, spintronic, and quantum devices.

Here, we develop lanthanum and a pyridine-based dicarboxamide organic linker (L) as a model system,  $LnL_3$ , to investigate the limit of X-ray detection on rare-earth-containing molecules at room temperature using synchrotron X-ray scanning tunneling microscopy (SX-STM). La is the lanthanide series’ first element with an empty  $4f$  shell with a  $[Xe]5d^16s^2$  configuration. The  $4f$  shell can become partially occupied due to the hybridization of the  $6s$ ,  $5d$ , and  $4f$  electrons. The local environments of the rare-earth ions in the molecules are important to investigate for designing molecule-based functional devices containing rare-earth metals.

Received: July 17, 2023

Revised: September 5, 2023

Published: October 2, 2023



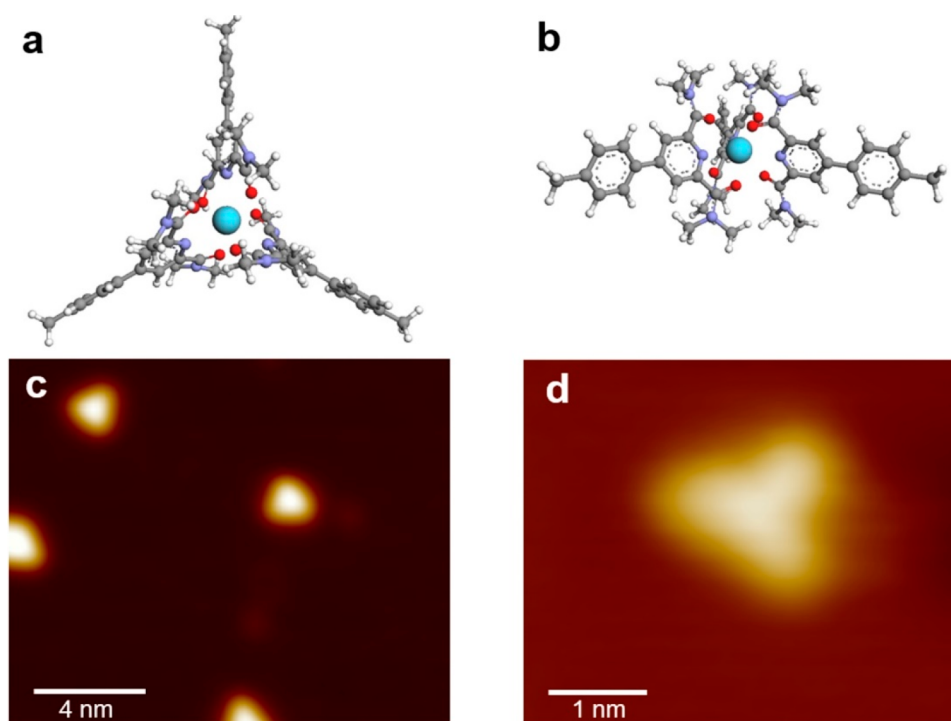


**Figure 1.** Structure of  $\text{La}(\text{pcam})_3$ . Models showing the (a) top view and (b) side view of  $\text{La}(\text{pcam})_3$ . (c) STM image displaying scattered  $\text{La}(\text{pcam})_3$  molecules on a  $\text{Cu}(111)$  surface at 5 K. (d) A zoomed-in STM image shows isolated  $\text{La}(\text{pcam})_3$  on  $\text{Cu}(111)$ .

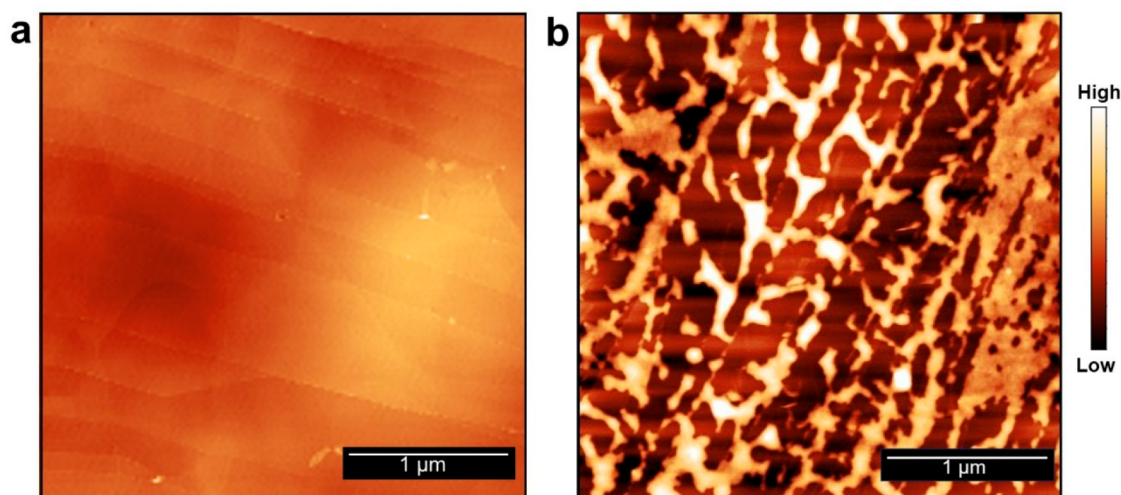


**Figure 2.** AFM characterizations. (a) AFM image of HOPG acquired after solvent-only deposition shows step-edge features of the substrate. (b) After drop-casting  $\text{La}(\text{pcam})_3$ , the areas covered by the molecules appear as protrusions (light-colored areas).

Synchrotron X-rays offer a powerful experimental method to simultaneously investigate elemental, chemical, and magnetic properties of materials.<sup>22–27</sup> Recently, the development of the SX-STM technique opened further possibilities for the X-ray characterization of materials down to the atomic limit at a low temperature of  $\sim 30$  K.<sup>22</sup> Here, we demonstrate that X-ray spectroscopy at atomic limits can be performed at room temperature. This work also provides a fundamental understanding of rare-earth ions coordinated with the molecules and will be useful for designing novel rare-earth molecular systems.<sup>28,29</sup>

## EXPERIMENTAL METHODS

To check the structure of the molecules, a  $\text{La}(\text{pcam})_3\text{-(CF}_3\text{SO}_3)_3$  salt was deposited from a custom-built Knudsen cell under an ultrahigh-vacuum (UHV) environment onto an atomically cleaned  $\text{Cu}(111)$  substrate. The sample was then transferred in situ to the scanning tunneling microscope (STM) chamber directly attached to the sample preparation chamber via a gate valve. STM imaging was performed at 5 K substrate temperature in UHV using a Createc GmbH STM system.

For the SX-STM measurements,  $\text{La}(\text{pcam})_3$  was dissolved in ethanol, and the solution was then drop-casted onto HOPG. SX-STM measurements were performed at the XTIP beamline located at sector 4-ID-E of the Advanced Photon Source and

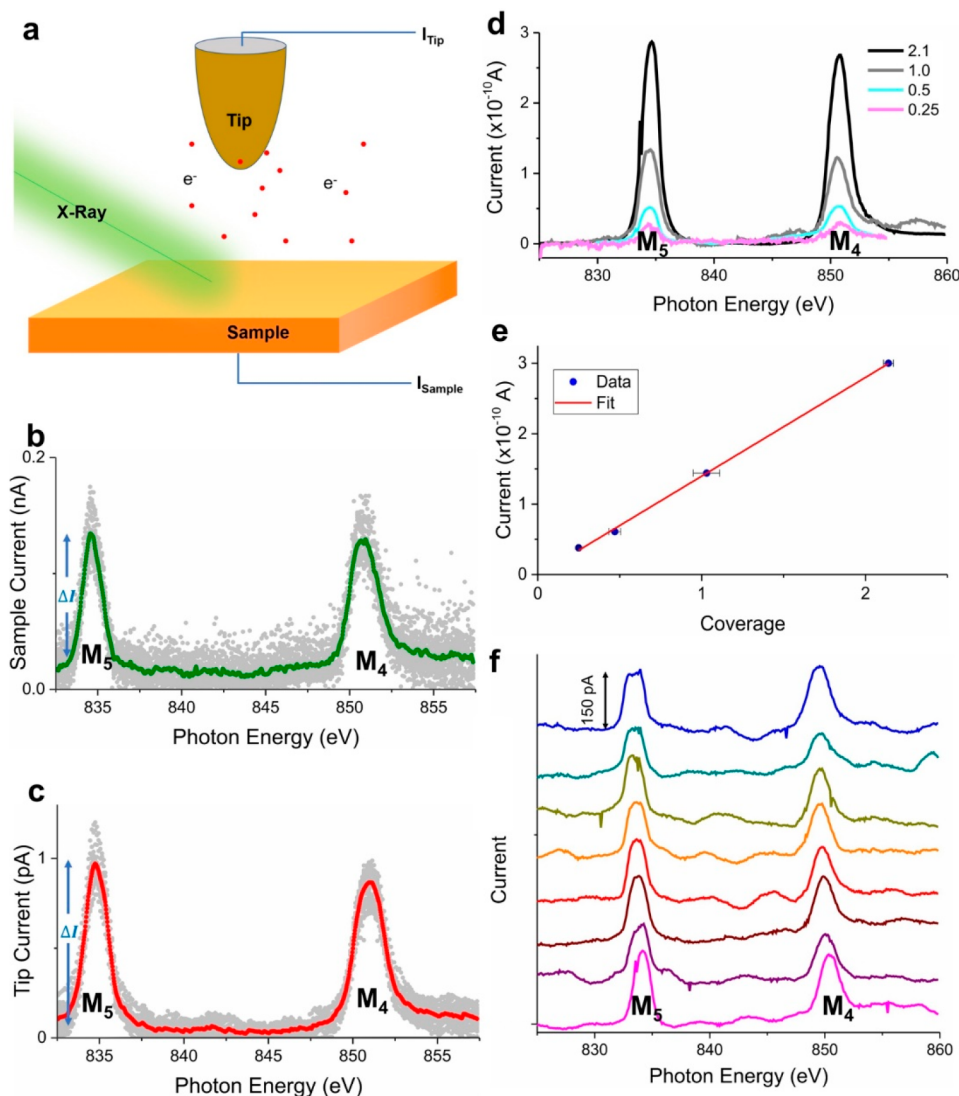


**Figure 3.** STM-XAS in the far-field regime. (a) Demonstration of SX-STM setup in the far-field regime where the tip is located  $\sim 5$  nm above the surface (out of the tunneling range). XAS spectra of the La  $M_{4,5}$  absorption edge are measured at sample channel (b) and tip channel (c). (d) XAS spectra for molecular coverages of 2.1, 1.0, 0.5, and 0.25 on HOPG. Here, the initial current for each curve is set to zero. (e) Current vs La(pcam)<sub>3</sub> coverage plot. (f) XAS spectra acquired at different sample locations show similar  $M_{4,5}$  peak intensities. In (b), (c), and (d), the initial current is set to zero. Here, the spectra are vertically shifted for clarity, and a vertical scale is included in the top spectrum.

the Center for Nanoscale Materials at the Argonne National Laboratory.<sup>30</sup> The SX-STM instrument was operated in UHV at room temperature. X-ray absorption spectra (XAS) were recorded with a step size of 0.1 eV at a resolving power of  $E/\Delta E$  of 4000.<sup>23</sup> For the experiments in the near-field, i.e., tunneling regime, the SX-STM tip was positioned at a fixed tip height above the sample at a tunneling distance ( $\sim 0.5$  nm) using a tunneling current set point of 100 pA and a bias voltage of  $-1$  V for data collection. Atomic force microscopy (AFM) measurements were performed in ScanAsyst mode using a Si cantilever (Veeco Multimode SPM, Bruker) at room temperature under ambient conditions.

## RESULTS AND DISCUSSION

The coordination complex used for the model study here is La(pcam)<sub>3</sub> [lanthanum(III) tris(2,6-pyridine carboxamide)]. La(pcam)<sub>3</sub> was synthesized from a solution of pcam and lanthanum(III) trifluoromethanesulfonate in acetonitrile, which was concentrated under reduced pressure (Supporting

Information). La(pcam)<sub>3</sub> has three equivalent ligand arms in a planar, distorted  $D_{3h}$  geometry with  $120^\circ$  angles between the nearest arms (Figure 1a). The La ion is well protected by the ligands (Figure 1a,b). The structures of the synthesized molecules were initially investigated by STM imaging. For this part of the study, a very low coverage of molecules was deposited by thermal evaporation onto an atomically clean Cu(111) surface in a UHV environment. The STM images acquired at a substrate temperature of 5 K show scattered molecules on the surface (Figure 1c). A close-up STM image (Figure 1d) reveals the expected triangular shape of the molecule, indicating that the molecule adsorbs in a planar geometry on this surface.

After successful synthesis and structural characterization of the La(pcam)<sub>3</sub> molecular system, we moved on to perform molecular-coverage-dependent SX-STM measurements. For the experiments, different La(pcam)<sub>3</sub> coverages were drop-cast from the solution onto a freshly cleaved highly ordered pyrolytic graphite (HOPG) substrate. For calibration, we first

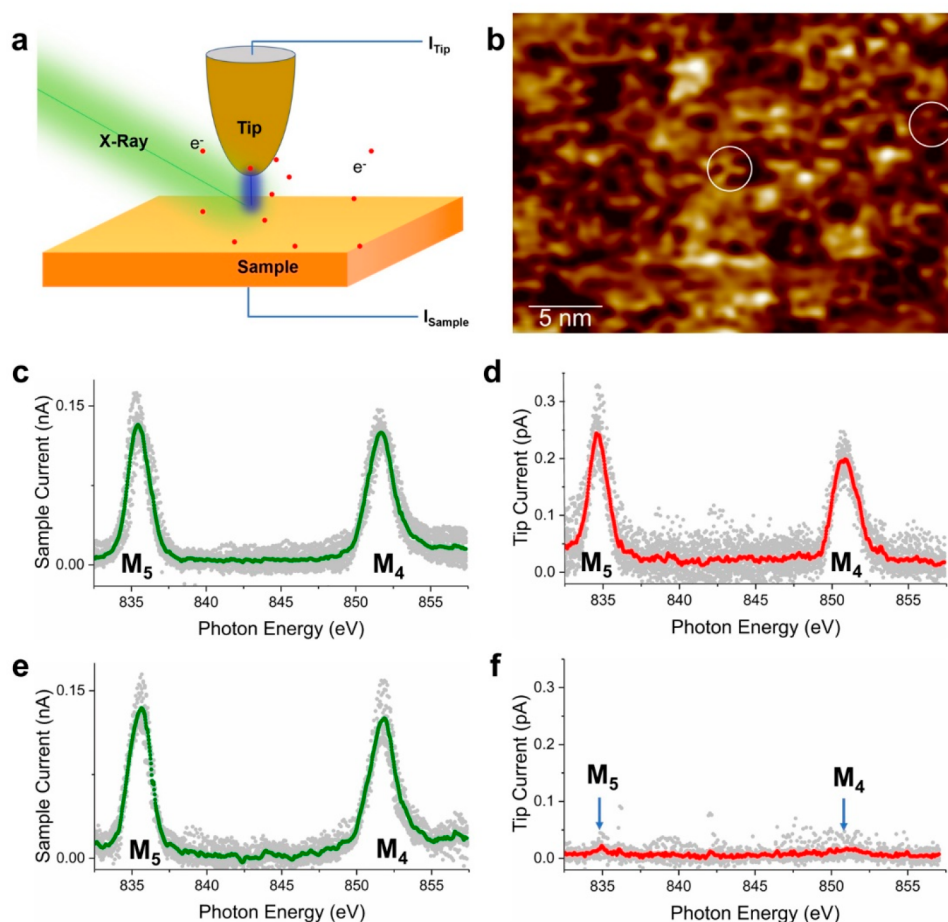


**Figure 4.** STM-XAS in the tunneling regime. (a) Demonstration of SX-STM setup in near-field (tunneling) regime. (b) STM image of  $\text{La}(\text{pcam})_3$  layer (0.96 coverage) drop-cast on HOPG measured by SX-STM. (c) STM-XAS spectra of  $\text{La}(\text{pcam})_3$  were measured at the sample channel when the tip signals showed the  $M_{4,5}$  edges. (d) STM-XAS spectra recorded at the tip channel showing cogent  $M_{4,5}$  edges in the tunneling range. (e) STM-XAS spectra of  $\text{La}(\text{pcam})_3$  were measured at the sample channel when the tip signals did not show the  $M_{4,5}$  edges. (f) Simultaneously recorded STM-XAS spectra together with (e) at the tip channel do not show cogent  $M_{4,5}$  edges in the tunneling range. The STM coaxial tip is held in the tunneling range  $I_t = 100$  pA and  $V_t = -1$  V. The green curves in (c) and (e) and the red curves in (d) and (f), the initial current is set to zero.

drop-cast solvent only onto the HOPG substrate and checked the surface with AFM imaging at ambient conditions. Large-area AFM images show no apparent solvent features, and clear step-edges of the surface can be observed (Figure 2a). After drop-casting a solvent containing  $\text{La}(\text{pcam})_3$ , the AFM images reveal relatively flat but brighter protruding regions partially covered across the surface (Figure 2b). The  $\text{La}(\text{pcam})_3$  coverage was estimated from large area AFM images (Figure 2 and Supporting Information). Here the height of the molecular islands can be 0.85–1.75 nm, which corresponds to one or two molecular-layer thicknesses (Supporting Information). Therefore, the height of the molecular islands is about 2.5–5 times higher than the step height of HOPG ( $\sim 0.34$  nm).

For our SX-STM experiments, a monochromatic synchrotron soft X-ray beam with a size of  $\sim 10 \mu\text{m} \times 10 \mu\text{m}$  cross section is passed through an X-ray chopper operating at 651 Hz, and then it is focused onto the tip–sample junction with an approximate angle of  $12.5^\circ$  from the surface plane. The X-ray chopper generates on and off cycles of the X-ray beam. When the X-ray beam is in the “off” position, an STM feedback loop is active for maintaining the tip height in the tunneling regime. X-ray excited tunneling electrons are collected using a

lock-in amplifier when the shutter is in the “on” position while maintaining the same tip height.<sup>22,23</sup> The frequency of the chopper is synchronized with the lock-in amplifier to extract the X-ray excited current (Supporting Information). X-ray absorption spectra are obtained by sweeping the photon energy over the La  $M_{4,5}$  edge region, from 832.5 to 857.5 eV.

In our SX-STM setup, the tip and sample photocurrents can be detected simultaneously (Figure 3a) using lock-in amplifiers connected to the tip and sample channels separately.<sup>22,31</sup> This enables a comparative study between the X-ray excited current signals simultaneously recorded at the separate tip and sample channels. Generally, two measurement modes of SX-STM, far-field, and near-field, can be realized.<sup>22,31</sup> In the far-field mode, the STM tip is held a few nanometers above the surface, out of the electron tunneling range (Figure 3a). When incident X-ray photons produce photoelectrons with energies higher than the work function of the sample, these electrons escape from the sample. In the soft X-ray regime, a significant number of Auger and secondary electrons are also generated during this process, which already occurs when core-level electrons are excited to the states between the Fermi level and the work function.<sup>32</sup> The photoexcitation of a core-level electron to either unoccupied states between the Fermi level and the work

function or to the continuum, i.e., above the work function, leaves a core hole that is subsequently filled by electrons from the higher orbits. During this process, Auger and secondary electrons are produced,<sup>22,32</sup> and electrons with sufficient energy escape the sample. A net current is generated by the electrons leaving the sample and is directly recorded by a lock-in amplifier at the sample channel (Figure 3a) as a function of incident photon energy (Figure 3b). The photocurrent signal recorded at the sample channel here is similar to the standard total electron yield (TEY) mode measurements.<sup>32,33</sup>

The sample channel measures the total number of electrons that are lost from the entire sample area illuminated by the X-ray beam, while the simultaneously recorded tip channel in the far-field mode captures only a fraction of these photoejected electrons.<sup>22</sup> By increasing the bias, the current captured at the tip increases because the photoejected electrons experience an electric field between the tip and the sample.<sup>23</sup> This effect is less pronounced at  $-1$  V compared to higher voltages, and thus a fixed  $-1$  V bias is used for all the measurements. Here, the utilization of a specialized coaxial tip enables the detection of a small fraction of photocurrent being captured by the tip (Figure 3c). The tip used in this study is formed by a tungsten (W) core, which is coated with a  $\text{SiO}_2$  insulating layer to prevent the collection of photoejected electrons at the side wall of the tip.<sup>22,24</sup> The outer wall of the coaxial tip is then coated with a titanium buffer layer and a gold layer, which is grounded to prevent capacitive charging. Only a range of 30–200 nm of the W tip apex is exposed, and thus it enables collecting photoelectrons locally.

Initially, we measure the  $M_{4,5}$  absorption edge of La to probe the d to f transitions in the TEY mode, i.e., recording the photocurrent at the sample channel only in the far-field mode (Figure 3b). Because of spin–orbit coupling, the  $M_5$  and  $M_4$  edges originate from  $3d_{5/2}$  and  $3d_{3/2}$  transitions to 4f orbitals, respectively.<sup>22,34</sup> The cogent peaks corresponding to  $M_5$  and  $M_4$  edges can be observed in both the sample and tip channels (Figure 3b,c). For one monolayer  $\text{La}(\text{pcam})_3$  coverage, the total current at the sample channel for the  $M_5$  peak is measured as  $\Delta I_{\text{sample}} = 134 \pm 31$  pA (Figure 3b), while the simultaneously recorded tip channel shows the maximum current for the  $M_5$  peak of  $\Delta I_{\text{tip}} = 1.0 \pm 0.2$  pA (Figure 3c). Thus, the total number of photoejected electrons captured in the tip channel is about 2 orders of magnitude less than the standard TEY mode of the sample channel.

Next, XAS spectra are acquired for various coverages of  $\text{La}(\text{pcam})_3$  on HOPG. Figure 3d shows the XAS spectra for  $\text{La}(\text{pcam})_3$  coverages of 2.1, 1.0, 0.5, and 0.25 monolayers (Supporting Information).

In XAS measurements, the photoejected current intensity in the TEY mode is known to saturate at larger film thickness above  $\sim 10$  nm depending on the type of materials in the film.<sup>35–37</sup> However, for very low coverages studied here with an island thickness of up to 1.7 nm, this saturation effect is not present or negligible. Consequently, the thickness of  $\text{La}(\text{pcam})_3$  islands here should not have any significant influence on the measured intensities of the  $M_5$  and  $M_4$  edge signals in the far-field. As expected, the maximum current at the  $M_5$  peak is progressively lower as the coverage decreases. Figure 3e shows the plot of the sample current measured at the  $M_5$  peak as a function of the molecular coverages. To confirm the uniformity of the molecule deposition, XAS spectra are measured at different locations on the sample (HOPG substrate of  $1 \text{ cm} \times 1 \text{ cm}$  area) by shifting the illuminated

area of  $10 \mu\text{m} \times 10 \mu\text{m}$  X-ray beam. The sample current signals corresponding to each X-ray illuminated area are plotted in Figure 3f, which reveal similar  $M_{4,5}$  absorption edge intensities indicating the uniformity of  $\text{La}(\text{pcam})_3$  concentration across the HOPG substrate after drop-casting.

Recently, X-ray spectroscopy measurements on an iron and a terbium atom using the SX-STM technique at low temperatures ( $\sim 30$  K) have been demonstrated.<sup>22</sup> The next step in this research direction is to determine whether similar single-atom X-ray detection can be realized at room temperature. For this measurement, the SX-STM is operated in the near-field, i.e., in the tunneling regime (Figure 4a) at room temperature. Here, the SX-STM tip approached the sample to a tunneling distance of  $\sim 0.5$  nm using  $-1$  V bias and 100 pA tunneling current. Then the images of the sample area to be examined are acquired in the STM imaging mode. The images (Figure 4b) reveal that the  $\text{La}(\text{pcam})_3$  molecules form a disordered layer on HOPG after drop-casting. Because of its disordered nature, it is difficult to resolve individual molecules, although the shape of the molecules can be identified occasionally (Figure 4b). This can be confirmed by comparison with the single-molecule images shown in Figure 1. For a conventional STM analysis, such a sample condition is challenging because the molecular layer may also include trapped solvent molecules. However, SX-STM probes core-level electrons, and only the La ions in the layer provide the desired signal at the characteristic photon energy. Thus, unlike STM, SX-STM is highly advantageous in the characterization of materials.

Next, the X-ray beam illuminates the tip–sample junction of the monolayer coverage sample, while the tip remains static above the molecular layer at a tunneling distance. Then the X-ray beam energy is ramped from 832.5 to 857.5 eV to cover the La  $M_{4,5}$  absorption edges. The X-ray excited tunneling electrons are simultaneously recorded at the tip and the sample channels by using separate lock-in amplifiers as before. For reproducibility, the STM-XAS spectra are collected every 6 nm across the sample for a total of  $150 \text{ nm} \times 24 \text{ nm}$  area. The results reveal two different sets of data (Figure 4c–f).

In the first set of spectra, both the sample and tip channels show cogent  $M_{4,5}$  edge signals of La (Figure 4c,d). Here, the sample channel in the tunneling regime contains contributions from both photoejected electrons and X-ray-excited tunneling electrons. It can be expressed as

$$I_{\text{total}} = I_{\text{sample}} + I_{\text{x-tunnel}} \quad (1)$$

Here,  $I_{\text{sample}}$  is the sample current purely composed of X-ray ejected electrons, which is produced by the entire X-ray illuminated area and is similar to the TEY mode, while  $I_{\text{x-tunnel}}$  is the X-ray excited tunneling current that is atomically localized. Note that the X-rays also excite electrons from the tip; however, the resultant current produced by the electrons leaving from the tip does not produce the La edge signal, and it only yields the background, which is subtracted (Supporting Information).

From Figure 3b, an  $I_{\text{sample}}$  value of  $0.134 \pm 0.031$  nA is measured, while  $I_{\text{x-tunnel}} = 0.23 \pm 0.07$  pA is directly determined from Figure 4d. Because the  $I_{\text{sample}}$  is about 3 orders of magnitude higher than  $I_{\text{x-tunnel}}$ ,  $I_{\text{total}} \approx I_{\text{sample}}$ . Thus, the recorded STM-XAS spectra for the sample channels in tunneling regime (Figure 4c,e) exhibit a similar intensity as shown in Figure 3b. However, due to the reduction of the solid angle for photoejected electrons, the tip captures only very few

photoejected electrons when it is in extreme proximity to the surface. Thus, the second set of spectra (Figure 4e,f), which is attributed as measured on the area where no La ion is present locally, reveal the  $M_{4,5}$  edge signals of La only at the sample channel, but there is no clear edge signal in the tip spectra although small traces of the edge signals may be discerned (indicated with arrows in Figure 4f).

Quantum tunneling is sensitive to the atomic position of the surface underneath the tip. It is known that the tunneling current exponentially decays with distance; thus, a change in 0.1 nm of tip height reduces the current approximately by 1 order of magnitude. Consequently, the top surface layer overwhelmingly contributes to the X-ray excited tunneling current while the contributions from the subsurface layers are negligible.<sup>24</sup> By considering the area of a single La(pcsm)<sub>3</sub> molecule, 1.73 nm<sup>2</sup>, where only one La atom is present, one should consider the contribution to the tunneling current by the La atoms from nearby molecules to be negligible. Thus, when the tip is directly located above a La ion in tunneling distance, the La edge signal can be obtained by the X-ray excited tunneling process while it is not the case when the tip is displaced from the La ion position. Such evidence has been recently demonstrated for low-temperature SX-STM measurements of isolated Fe and Tb atoms coordinated to molecular hosts where the Fe and Tb edge signals can be observed only when the tip is directly located above the atomic positions in a tunneling distance; otherwise, their edge signals are absent.<sup>22</sup> This suggests that the observed La signal at the tip current in the tunneling regime is contributed by an individual La ion.

As discussed above, the far-field sample current is similar to a TEY mode measurement, and the current intensity depends on the number of La atoms in the molecular film. The utilization of a specialized coaxial tip reduces the tip current in the far-field by about 2 orders of magnitude as compared to the sample channel. However, in the near-field regime, the current in the tip channel is predominantly produced by the X-ray excited tunneling process, and it is inherently limited by the available states of a single atom responsible for the tunneling channel. Thus, unlike the tip current intensity in the far-field, the tip current in the near-field is independent of the molecular coverage. The current at the  $M_5$  edge in the tip channel in the near-field is  $0.23 \pm 0.07$  pA (Figure 4d). This value agrees well with the recently reported X-ray excited current values of individual Fe and Tb atoms, 0.3 and 0.1–0.2 pA, at their  $L_3$  and  $M_5$  edges, respectively.<sup>22</sup> This further confirms that the observed signal is produced from a single La ion.

## CONCLUSIONS

We used the SX-STM technique to characterize a rare-earth-based molecular system at room temperature. By extending measurements with SX-STM from the far-field to the near-field regime, we show that X-ray characterization can be performed down to a single La ion via the X-ray excited tunneling process at room temperature. The measurements were performed on molecular films drop-casted from solution, and thus, it is challenging to perform atomically resolved structural characterization using only the conventional scanning probe techniques. In contrast, the SX-STM technique proves to be a robust characterization method because it utilizes core-level excitations of a target element and therefore is less impacted by potential surface contaminations. The SX-STM technique also allows probing the chemical environment of the materials. Both far-field and near-field (tunneling regime) measurements

do not show significant changes in the profile shapes and energetic positions of the La  $M_5$  and  $M_4$  peaks indicating that La ion is well protected in the pcsm cage. This is in accordance with previous observations of Eu, and Tb ions in similar pcsm cages on metallic substrates, where the near-edge X-ray absorption fine structure spectra measured by SX-STM reveal that the rare-earth ions are well protected by the surrounding organic ligands from the environment.<sup>14,22</sup> This work provides a fundamental understanding of the local environment of rare-earth ions caged inside molecular scaffolds and will pave the way for investigating novel rare-earth molecular systems using synchrotron X-rays at room temperature at the ultimate single atom limit.

## ASSOCIATED CONTENT

### Supporting Information

The Supporting Information is available free of charge at <https://pubs.acs.org/doi/10.1021/acs.jpcc.3c04806>.

Generalities; preparation of pcsm (3) and [La(pcsm)<sub>3</sub>](CF<sub>3</sub>SO<sub>3</sub>)<sub>3</sub>; characterization of [La(pcsm)<sub>3</sub>](CF<sub>3</sub>SO<sub>3</sub>)<sub>3</sub> (4) and precursors; atomic force microscopy characterization of La(pcsm)<sub>3</sub> drop-casted onto HOPG; coverage calibration; XAS plots before and after subtracting the background; references (PDF)

## AUTHOR INFORMATION

### Corresponding Authors

Sarah Wiegold – Advanced Photon Source, Argonne National Laboratory, Lemont, Illinois 60439, United States; Email: [swiegold@anl.gov](mailto:swiegold@anl.gov)

Saw Wai Hla – Nanoscience & Technology Division, Argonne National Laboratory, Lemont, Illinois 60439, United States; Nanoscale & Quantum Phenomena Institute, and Department of Physics & Astronomy, Ohio University, Athens, Ohio 45701, United States; Email: [hla@ohio.edu](mailto:hla@ohio.edu)

### Authors

Nozomi Shirato – Nanoscience & Technology Division, Argonne National Laboratory, Lemont, Illinois 60439, United States

Xinyue Cheng – Department of Chemistry and Biochemistry, Ohio University, Athens, Ohio 45701, United States

Kyaw Zin Latt – Nanoscience & Technology Division, Argonne National Laboratory, Lemont, Illinois 60439, United States

Daniel Trainer – Nanoscience & Technology Division, Argonne National Laboratory, Lemont, Illinois 60439, United States

Richard Sottie – Nanoscale & Quantum Phenomena Institute, and Department of Physics & Astronomy, Ohio University, Athens, Ohio 45701, United States; [orcid.org/0000-0002-2453-0124](https://orcid.org/0000-0002-2453-0124)

Daniel Rosenmann – Nanoscience & Technology Division, Argonne National Laboratory, Lemont, Illinois 60439, United States

Eric Masson – Department of Chemistry and Biochemistry, Ohio University, Athens, Ohio 45701, United States; [orcid.org/0000-0001-9387-4783](https://orcid.org/0000-0001-9387-4783)

Volker Rose – Advanced Photon Source, Argonne National Laboratory, Lemont, Illinois 60439, United States

Complete contact information is available at: <https://pubs.acs.org/doi/10.1021/acs.jpcc.3c04806>

## Notes

The authors declare no competing financial interest.

## ACKNOWLEDGMENTS

We acknowledge financial support from the U.S. Department of Energy, Office of Science, Office of Basic Energy Sciences, Materials Science and Engineering Division. Work performed at the Center for Nanoscale Materials and Advanced Photon Source, both U.S. Department of Energy Office of Science User Facilities, was supported by the U.S. DOE, Office of Basic Energy Sciences, under Contract DE-AC02-06CH11357.

## REFERENCES

- (1) Zheng, W.; Huang, P.; Gong, Z.; Tu, D.; Xu, J.; Zou, Q.; Li, R.; You, W.; Bünzli, J.-C. G.; Chen, X. Near-Infrared-Triggered Photon Upconversion Tuning in All-Inorganic Cesium Lead Halide Perovskite Quantum Dots. *Nat. Commun.* **2018**, *9* (1), 3462.
- (2) Schoenauer Sebag, M.; Hu, Z.; de Oliveira Lima, K.; Xiang, H.; Gredin, P.; Mortier, M.; Billot, L.; Aigouy, L.; Chen, Z. Microscopic Evidence of Upconversion-Induced Near-Infrared Light Harvest in Hybrid Perovskite Solar Cells. *ACS Appl. Energy Mater.* **2018**, *1* (8), 3537–3543.
- (3) Wen, S.; Zhou, J.; Zheng, K.; Bednarkiewicz, A.; Liu, X.; Jin, D. Advances in Highly Doped Upconversion Nanoparticles. *Nat. Commun.* **2018**, *9* (1), 2415.
- (4) Zhou, D.; Liu, D.; Pan, G.; Chen, X.; Li, D.; Xu, W.; Bai, X.; Song, H. Cerium and Ytterbium Codoped Halide Perovskite Quantum Dots: A Novel and Efficient Downconverter for Improving the Performance of Silicon Solar Cells. *Adv. Mater.* **2017**, *29* (42), 1704149.
- (5) Luo, X.; Ding, T.; Liu, X.; Liu, Y.; Wu, K. Quantum-Cutting Luminescent Solar Concentrators Using Ytterbium-Doped Perovskite Nanocrystals. *Nano Lett.* **2019**, *19* (1), 338–341.
- (6) Hedges, M. P.; Longdell, J. J.; Li, Y.; Sellars, M. J. Efficient Quantum Memory for Light. *Nature* **2010**, *465* (7301), 1052–1056.
- (7) Saglamyurek, E.; Sinclair, N.; Jin, J.; Slater, J. A.; Oblak, D.; Bussi eres, F.; George, M.; Ricken, R.; Sohler, W.; Tittel, W. Broadband Waveguide Quantum Memory for Entangled Photons. *Nature* **2011**, *469* (7331), 512–515.
- (8) Zhong, T.; Kindem, J. M.; Bartholomew, J. G.; Rochman, J.; Craiciu, I.; Verma, V.; Nam, S. W.; Marsili, F.; Shaw, M. D.; Beyer, A. D.; et al. Optically Addressing Single Rare-Earth Ions in a Nanophotonic Cavity. *Phys. Rev. Lett.* **2018**, *121* (18), 183603.
- (9) Dibos, A. M.; Raha, M.; Phenicie, C. M.; Thompson, J. D. Atomic Source of Single Photons in the Telecom Band. *Phys. Rev. Lett.* **2018**, *120* (24), 243601.
- (10) Zhong, M.; Hedges, M. P.; Ahlefeldt, R. L.; Bartholomew, J. G.; Beavan, S. E.; Wittig, S. M.; Longdell, J. J.; Sellars, M. J. Optically Addressable Nuclear Spins in a Solid with a Six-Hour Coherence Time. *Nature* **2015**, *517* (7533), 177–180.
- (11) de Riedmatten, H.; Afzelius, M.; Staudt, M. U.; Simon, C.; Gisin, N. A Solid-State Light-Matter Interface at the Single-Photon Level. *Nature* **2008**, *456* (7223), 773–777.
- (12) Böttger, T.; Thiel, C. W.; Cone, R. L.; Sun, Y. Effects of Magnetic Field Orientation on Optical Decoherence in Er<sup>3+</sup>:Y<sub>2</sub>SiO<sub>5</sub>. *Phys. Rev. B* **2009**, *79* (11), 115104.
- (13) Sun, Y.; Thiel, C. W.; Cone, R. L.; Equall, R. W.; Hutcheson, R. L. Recent Progress in Developing New Rare Earth Materials for Hole Burning and Coherent Transient Applications. *J. Lumin.* **2002**, *98* (1), 281–287.
- (14) Ajayi, T. M.; Singh, V.; Latt, K. Z.; Sarkar, S.; Cheng, X.; Premarathna, S.; Dandu, N. K.; Wang, S.; Movahedifar, F.; Wiegold, S.; et al. Atomically Precise Control of Rotational Dynamics in Charged Rare-Earth Complexes on a Metal Surface. *Nat. Commun.* **2022**, *13*, 6305.
- (15) Wong, H.-Y.; Lo, W.-S.; Yim, K.-H.; Law, G.-L. Chirality and Chiroptics of Lanthanide Molecular and Supramolecular Assemblies. *Chem.* **2019**, *5* (12), 3058–3095.
- (16) Barry, D. E.; Caffrey, D. F.; Gunnlaugsson, T. Lanthanide-Directed Synthesis of Luminescent Self-Assembly Supramolecular Structures and Mechanically Bonded Systems from Acyclic Coordinating Organic Ligands. *Chem. Soc. Rev.* **2016**, *45* (11), 3244–3274.
- (17) Wasielewski, M. R.; Forbes, M. D. E.; Frank, N. L.; Kowalski, K.; Scholes, G. D.; Yuen-Zhou, J.; Baldo, M. A.; Freedman, D. E.; Goldsmith, R. H.; Goodson, T.; et al. Exploiting Chemistry and Molecular Systems for Quantum Information Science. *Nature Reviews Chemistry* **2020**, *4* (9), 490–504.
- (18) Hamacek, J.; Poggiali, D.; Zebret, S.; Aroussi, B. E.; Schneider, M. W.; Mastalerz, M. Building Large Supramolecular Nanocapsules with Europium Cations. *Chem. Commun.* **2012**, *48* (9), 1281–1283.
- (19) Yan, L.-L.; Tan, C.-H.; Zhang, G.-L.; Zhou, L.-P.; Bünzli, J.-C.; Sun, Q.-F. Stereocontrolled Self-Assembly and Self-Sorting of Luminescent Europium Tetrahedral Cages. *J. Am. Chem. Soc.* **2015**, *137* (26), 8550–8555.
- (20) Kotova, O.; Comby, S.; Pandurangan, K.; Stomeo, F.; O'Brien, J. E.; Feeney, M.; Peacock, R. D.; McCoy, C. P.; Gunnlaugsson, T. The Effect of the Linker Size in C<sub>2</sub>-Symmetrical Chiral Ligands on the Self-Assembly Formation of Luminescent Triple-Stranded Di-Metallic Eu(III) Helicates in Solution. *Dalton Trans.* **2018**, *47* (35), 12308–12317.
- (21) Delor, M.; Archer, S. A.; Keane, T.; Meijer, A. J. H. M.; Sazanovich, I. V.; Greetham, G. M.; Towrie, M.; Weinstein, J. A. Directing the Path of Light-Induced Electron Transfer at a Molecular Fork Using Vibrational Excitation. *Nat. Chem.* **2017**, *9* (11), 1099–1104.
- (22) Ajayi, T. M.; Shirato, N.; Rojas, T.; Wiegold, S.; Cheng, X.; Latt, K. Z.; Trainer, D. J.; Dandu, N. K.; Li, Y.; Premarathna, S. Characterization of just one atom using synchrotron x-rays. *Nature* **2013**, *618*, 69–73.
- (23) Rose, V.; Wang, K.; Chien, T.; Hiller, J.; Rosenmann, D.; Freeland, J. W.; Preissner, C.; Hla, S. W. Synchrotron X-Ray Scanning Tunneling Microscopy: Fingerprinting Near to Far Field Transitions on Cu(111) Induced by Synchrotron Radiation. *Adv. Funct. Mater.* **2013**, *23* (20), 2646–2652.
- (24) Shirato, N.; Cummings, M.; Kersell, H.; Li, Y.; Stripe, B.; Rosenmann, D.; Hla, S. W.; Rose, V. Elemental Fingerprinting of Materials with Sensitivity at the Atomic Limit. *Nano Lett.* **2014**, *14* (11), 6499–6504.
- (25) Chang, H.; Shirato, N.; Zhang, Y.; Hoffman, J.; Rosenmann, D.; Freeland, J. W.; Bhattacharya, A.; Rose, V.; Hla, S. W. X-Ray Magnetic Circular Dichroism and Near-Edge X-Ray Absorption Fine Structure of Buried Interfacial Magnetism Measured by Using a Scanning Tunneling Microscope Tip. *Appl. Phys. Lett.* **2018**, *113* (6), 061602.
- (26) Wiegold, S.; Cope, E. M.; Moller, G.; Shirato, N.; Guzelurk, B.; Rose, V.; Nienhaus, L. Stressing Halide Perovskites with Light and Electric Fields. *ACS Energy Lett.* **2022**, *7*, 2211–2218.
- (27) Wiegold, S.; Shirato, N.; Rose, V.; Nienhaus, L. Investigating the Effect of Electric Fields on Lead Halide Perovskites by Scanning Tunneling Microscopy. *J. Appl. Phys. Phys.* **2020**, *128*, 084703.
- (28) Emmanuele, R.; Maciejczyk, M.; Smith, A.; Cheng, X.; Masson, E.; Gosztola, D. J.; Hla, S.-W.; Robertson, N.; Ma, X. Microcavity-Modified Emission from Rare-Earth Ion-Based Molecular Complexes. *ACS Photonics* **2022**, *9* (7), 2315–2321.
- (29) Yim, K.-H.; Yeung, C.-T.; Wong, H.-Y.; Law, G.-L. Structural Variation of Self-Assembled Lanthanide Supramolecular Complexes Induced by Reaction Conditions. *Inorg. Chem. Front.* **2021**, *8* (12), 2952–2964.
- (30) Rose, V.; Shirato, N.; Bartlein, M.; Deriy, A.; Ajayi, T.; Rosenmann, D.; Hla, S. W.; Fisher, M.; Reininger, R. XTIP - the World's First Beamline Dedicated to the Synchrotron X-Ray Scanning Tunneling Microscopy Technique. *Journal of Synchrotron Radiation* **2020**, *27* (3), 836–843.
- (31) Kersell, H.; Shirato, N.; Cummings, M.; Chang, H.; Miller, D.; Rosenmann, D.; Hla, S. W.; Rose, V. Detecting Element Specific Electrons from a Single Cobalt Nanocluster with Synchrotron X-Ray Scanning Tunneling Microscopy. *Appl. Phys. Lett.* **2017**, *111* (10), 103102.

(32) Abbate, M.; Goedkoop, J. B.; de Groot, F. M. F.; Grioni, M.; Fuggle, J. C.; Hofmann, S.; Petersen, H.; Sacchi, M. Probing Depth of Soft X-ray Absorption Spectroscopy Measured in Total-Electron-Yield Mode. *Surf. Interface Anal.* **1992**, *18* (1), 65–59.

(33) Frazer, B. H.; Gilbert, B.; Sonderegger, B. R.; De Stasio, G. The Probing Depth of Total Electron Yield in the Sub-keV Range: TEY-XAS and X-PEEM. *Surf. Sci.* **2003**, *537* (1–3), 161–167.

(34) Thole, B. T.; van der Laan, G.; Fuggle, J. C.; Sawatzky, G. A.; Karnatak, R. C.; Esteve, J.-M. 3d X-Ray-Absorption Lines and the 3d<sup>9</sup>4f<sup>n</sup>+1 Multiplets of the Lanthanides. *Phys. Rev. B* **1985**, *32* (8), 5107–5118.

(35) Nakajima, R.; Stohr, J.; Idzerda, Y. U. Electron-Yield Saturation Effects in L-Edge X-ray Magnetic Circular Dichroism Spectra of Fe, Co, and Ni. *Phys. Rev. B* **1999**, *59* (9), 6421–6429.

(36) Aksoy, F.; Akgul, G.; Ufuktepe, Y.; Nordlund, D. Thickness Dependence of the L<sub>2,3</sub> Branching Ratio of Cr Thin Films. *J. Alloy. Compd.* **2010**, *508* (2), 233–237.

(37) Gota, S.; Gautier-Soyer, M.; Sacchi, M. Fe 2p Absorption in Magnetic Oxides: Quantifying Angular-Dependent Saturation Effects. *Phys. Rev. B* **2000**, *62* (7), 4187–4190.